Electrochemistry Communications 109 (2019) 106604

Contents lists available at ScienceDirect

Electrochemistry Communications

journal homepage: www.elsevier.com/locate/elecom

The effects of $BaTiO_3$ nanodots density support on epitaxial $LiCoO_2$ thin-film for high-speed rechargeability

Sou Yasuhara[a], Shintaro Yasui[a,*], Takashi Teranishi[b], Yumi Yoshikawa[b], Tomoyasu Taniyama[a,c], Mitsuru Itoh[a,*]

[a] Laboratory for Materials and Structures, Tokyo Institute of Technology, Yokohama 226-8503, Japan
[b] Graduate School of Natural Science and Technology, Okayama University, Okayama 700-8530, Japan
[c] Department of Physics, Nagoya University, Nagoya 464-8601, Japan

ARTICLE INFO

Keywords:
High speed chargeability
Nanodots
Density
Dielectrics
$LiCoO_2$

ABSTRACT

$LiCoO_2$ (LCO) is one of the most promising cathode materials for Li ion batteries (LIBs). However, LCO shows a rate-limiting step of Li^+ migration between electrode and electrolyte interfaces, requiring LIBs to be charged under low-current conditions. For next generation batteries, it will be necessary to meet the demand for a shorter charging-time. We investigated a support method for the LCO surface to improve high C-rate performance, and revealed that the Li^+ intercalation/de-intercalation reaction into/from LCO was accelerated by the introduction of a $BaTiO_3$-LCO-electrolyte interface (triple-phase interface; TPI), due to the electric field concentration near the TPI. In this report, we investigate the dependence of high C-rate performance on the density of surface $BaTiO_3$ nanodots using epitaxial $LiCoO_2$ thin films created via pulsed laser deposition (PLD). As the number of nanodots increased, so did discharge capacity at 50C, becoming saturated at surface coverage over 22%. However, at 100C, the discharge capacity decreased at surface coverage over 40%. These results indicate that coalescence of nanodots reduces not only the TPI length but also the electrochemically active range at quite high C-rate. Therefore, we infer that optimal surface coverage should be varied depending on the C-rate.

1. Introduction

Li ion batteries (LIBs) [1,2] have been commercialized worldwide as a portable electric storage device because of superior properties such as high working voltage and large specific capacity. However, LIBs still have several problems, the most serious one is charge/discharge speed. $LiCoO_2$ (LCO) is the most well-known material used in LIB cathodes [3], with a charge reaction that can be written as the following equation: $LiCoO_2 \rightarrow xLi^+ + xe^- + Li_{1-x}CoO_2$. During the charging process, the Li ion (Li^+) is de-inserted from LCO. Due to the high resistance of Li^+ migration between electrode and electrolyte [4], the charging speed is limited. There is, however, a strong demand for higher speed rechargeable batteries. Accordingly, it is necessary to enhance the Li^+ migration between electrolyte and electrode.

Three promising approaches have been reported in the effort to improve high-speed rechargeability: searching for a cathode material with low interfacial resistance [5,6]; miniaturizing electrode materials [7]; and determining a way to support the material on the surface of the electrode [8–10]. Of these, the surface-supporting method is attractive in that it can be combined with other methods, although the mechanism of how to improve the high speed rechargeability remains unclear. Note that investigating the mechanism of this method is a promising way to fulfill the demands for next-generation LIBs, because high-speed rechargeability could be achieved by introducing critical supporting materials, optimal surface coverage, ideal shape of supporting material, etc.

In our previous work, we investigated the mechanism of a method to support the surface using $BaTiO_3$ (BTO) nanodots deposited on a LCO epitaxial thin film, and revealed that Li^+ migration could be accelerated near the BTO-LCO-electrolyte (triple-phase interface, TPI) caused by the electric field concentration [11,12]. Based on this finding, we expected that we could easily vary the enhancement of high C-rate performance by altering the surface coverage of supporting material. In this letter, we prepared BTO nanodots deposited on LCO epitaxial thin films at various degrees of surface coverage by controlling the deposition time of the nanodots. The prepared films were characterized by XRD and SEM. Charge-discharge measurements were performed after assembling 2032 coin-type measurements cell. The finite element method for calculation of a surface electric field was carried out using ANSYS-HFSS ver. 18.1.

* Corresponding authors.
E-mail addresses: yasui.s.aa@m.titech.ac.jp (S. Yasui), itoh.m.aa@m.titech.ac.jp (M. Itoh).

https://doi.org/10.1016/j.elecom.2019.106604
Received 1 October 2019; Received in revised form 6 November 2019; Accepted 6 November 2019
Available online 07 November 2019

2. Experimental

All thin films were prepared by the pulsed laser deposition (PLD) method with a 4th harmonic Nd: YAG laser (266 nm). First, an $SrRuO_3$ (SRO) layer (50-nm thick) was prepared on a (100)$SrTiO_3$ (STO) substrate as a current collector. Next, an LCO layer (150-nm thick) was deposited on the SRO/STO substrate using a lithium-excess $Li_{1.2}CoO_2$ target to compensate the lack of Li in the film due to the high vapor pressure during deposition [13]. In this paper, we designate this LCO/SRO/STO film as Bare. Subsequently, BTO nanodots were grown on the Bare surface under the following conditions: $p(O_2)$ of 2 Torr and substrate temperature of 630 °C, where BTO is known to show an island growth Volmer-Weber (VW) mode [11]. We chose deposition times of 30 s, 2 min, 4 min, and 6 min to attain BTO nanodots/Bare film with different surface coverage; hereafter referred to as Dot-30sec, Dot-2 min, Dot-4 min and Dot-6 min, respectively.

3. Results and discussion

X-ray diffraction (XRD) measurements were performed using Rigaku Smartlab to characterize crystal structure of the prepared thin films. The out-of-plane XRD patterns of fabricated thin films are shown in Fig. 1. In this figure, the reflection index of SRO was written with a pseudo-cubic structure, and the subscript "c" represents the cubic. The results indicate that the LCO(104)//SRO(001)$_c$//STO(001) relationship was obtained, and there were no impurity phases in the films. Note that no diffractions of BTO were detected by XRD because the amount of deposited BTO was quite small in all films. To observe the BTO nanodots, scanning electron microscopy (SEM) measurements were carried out using Hitachi S-4800. Surface SEM images of fabricated thin films are shown in Fig. 2(a–e). With increasing deposition time, there was an evident increase in the number of white dots in Dot-2 min, Dot-4 min, and Dot-6 min, although no dots could be observed in Bare and Dot-30sec. These white dots correspond to BTO nanodots. The dot diameter was estimated to be about 10 nm. Surface coverage of Dot-2 min, Dot-4 min and Dot-6 min was calculated to be 22%, 31% and 40%, respectively (see inset of Fig. 2(f)). Unfortunately, we could not determine the surface coverage of Dot-30sec because the BTO nanodots were not visible in SEM image. Number of dots in a 100 nm × 100 nm selected area of each film was counted, and the results are presented in Fig. 2(f). The dashed diagonal red line in the figure is just an eye guide. The nonlinear relation between dot number and deposition time is clear, indicating that coalescence occurs between BTO nanodots with increasing deposition time. TPI-length in a selected area of 100 nm × 100 nm is shown in Fig. 2(g). The TPI-length of Dot-6 min was shorter than that of Dot-4 min.

Next a 2032-type coin cell was assembled in an Ar-filled glove box

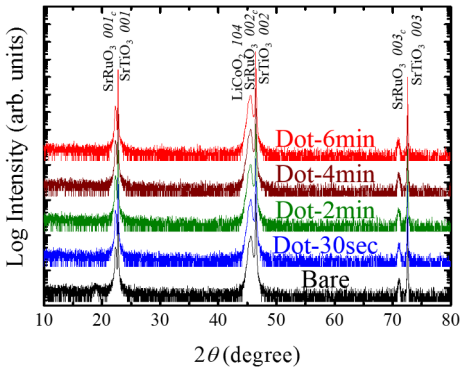

Fig. 1. Out-of-plane XRD patterns of Bare (black), Dot-30sec (blue), Dot-2 min (green), Dot-4 min (dark-red) and Dot-6 min (bright-red). (For interpretation of the references to colour in this figure legend, the reader is referred to the web version of this article.)

using the fabricated thin film as the cathode, Li metal as the anode, and $LiPF_6$ (Ethylene carbonate [EC]: Diethyl carbonate [DEC]) as the electrolyte. Charge-discharge measurements of the cell were performed as the C-rate was gradually increased from 1C to 2C, 5C, 10C, 20C, 50C, 100C, and then finally returned to 1C(2nd). The discharge capacities are shown in Fig. 3(a). Unstable discharge capacities at initial 1C were observed in all films due to SEI formation process, side reaction and unknown contributions. However, they began to be stable after couple of cycling (actually, stable at 2C), therefore break-in cycle might not be affected higher rate performance.

All prepared cells continued to work even in the 40th cycle at 1C(2nd). These results indicated that none of the samples were broken down. However, some samples showed almost null discharge capacity at 50C or 100C. The Bare sample worked until 20C, but did not work at 50C or 100C. On the other hand, samples with deposited BTO showed different trends. To evaluate the effect of dot density, the discharge capacity at 20C, 50C and 100C were normalized by average capacity at 1C(2nd), and replotted as a function of dot deposition time. Fig. 3(b) shows the normalized discharge capacities. At 20C and 50C, as dot-deposition time increased, so did the normalized discharge capacities, reaching saturation above the dot deposition time of 2 min. On the contrary, at 100C, Dot-2 min and Dot-4 min showed 27% of normalized discharge capacities, while Dot-6 min showed almost null normalized discharge capacity. These results indicate that optimal dot-density varies depending on the C-rate. To discuss this trend in more detail, we evaluated the cell resistances.

The resistance of cells, R_{cell}, can be calculated from the contribution of IR drop estimated by the plateau voltage of LCO charge curves. The plateau voltage, V_M, can be expressed by the following equation:

$$V_M = V_{LCO} + IR_{cell}$$

where V_{LCO} and I are the theoretical reaction voltage of LCO and the applied current, respectively. The plateau voltage corresponds to that where the differential of capacity by voltage (dQ/dV) in charge curves shows a maximum value. Here, we supposed V_{LCO} is independent of the C-rate and the polarization of charge curve corresponds to the over voltage of IR_{cell}. The over voltage of IR_{cell} can be evaluate with dQ/dV curves in different C-rate. The calculated R_{cell} values of Bare, Dot-30sec, Dot-2 min, Dot-4 min and Dot-6 min were 2600 Ω, 730 Ω, 550 Ω, 580 Ω, and 610 Ω, respectively. The R_{cell} value decreased with increasing dot deposition time, t, in the region $t < 2$ min. In addition, R_{cell} value took almost the same value in the region $t > 2$ min. The rate-limiting step of lithium insertion/de-insertion into/from LCO thin film has been reported to be the charge-transfer step consisting of Li^+ migration across the electrode and electrolyte interfaces, the electron supply, and the Li^+ solvation reaction with the PF_6^- ions [14,15]. These results imply that the surface support method reduced the resistance of Li^+ migration across the electrode-electrolyte interface, resulting in an enhanced discharge capacity at 50C and saturation for surface coverage above ~20%. In the case of 100C, Dot-6 min showed a decrease of normalized discharge capacity (Fig. 3(b)). This decrease might be due to limiting contributions other than the Li^+ migration between electrode and electrolyte interfaces, because R_{cell} values of Dot-6 min were almost the same as those of Dot-2 min and Dot-4 min.

To infer the other limiting contribution, we focused on the Li^+ diffusion process. In this process, three resistance factors combine to create overall resistance: (1) Li^+ migration between electrode-electrolyte interfaces (R_{ct}); (2) inner-diffusion limitation (R_{diff}); and (3) Li^+ diffusion in electrolyte (R_{elec}). Generally, R_{elec} will have quite a low value in the case of a liquid electrolyte. On the other hand, the R_{diff} could vary with the Li concentration in LCO [16]. When applying large current (i.e., high C-rate) to the electrode, the Li^+ supply by inner diffusion is insufficient, and the LCO surface voltage would reach the cutoff voltage. The charge/discharge process might have finished even though some Li concentration gradient was remaining. As previously reported, Li^+ could not penetrate the BTO layer [11]. Thereby, the area

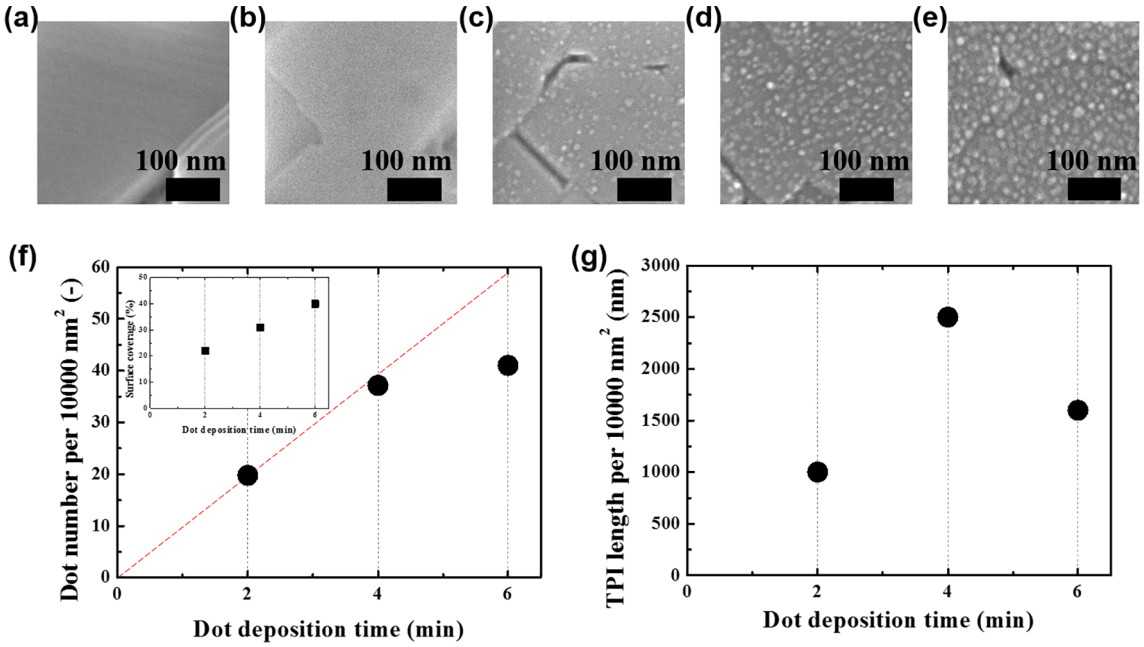

Fig. 2. Surface SEM images of Bare (a), Dot-30sec (b), Dot-2 min (c), Dot-4 min (d) and Dot-6 min (e). Density of dots per area of 100 nm × 100 nm *vs.* dot deposition time (f). Surface coverage *vs.* dot deposition time in the inset of (f). TPI-length per area of 100 nm × 100 nm *vs.* dot deposition time (g).

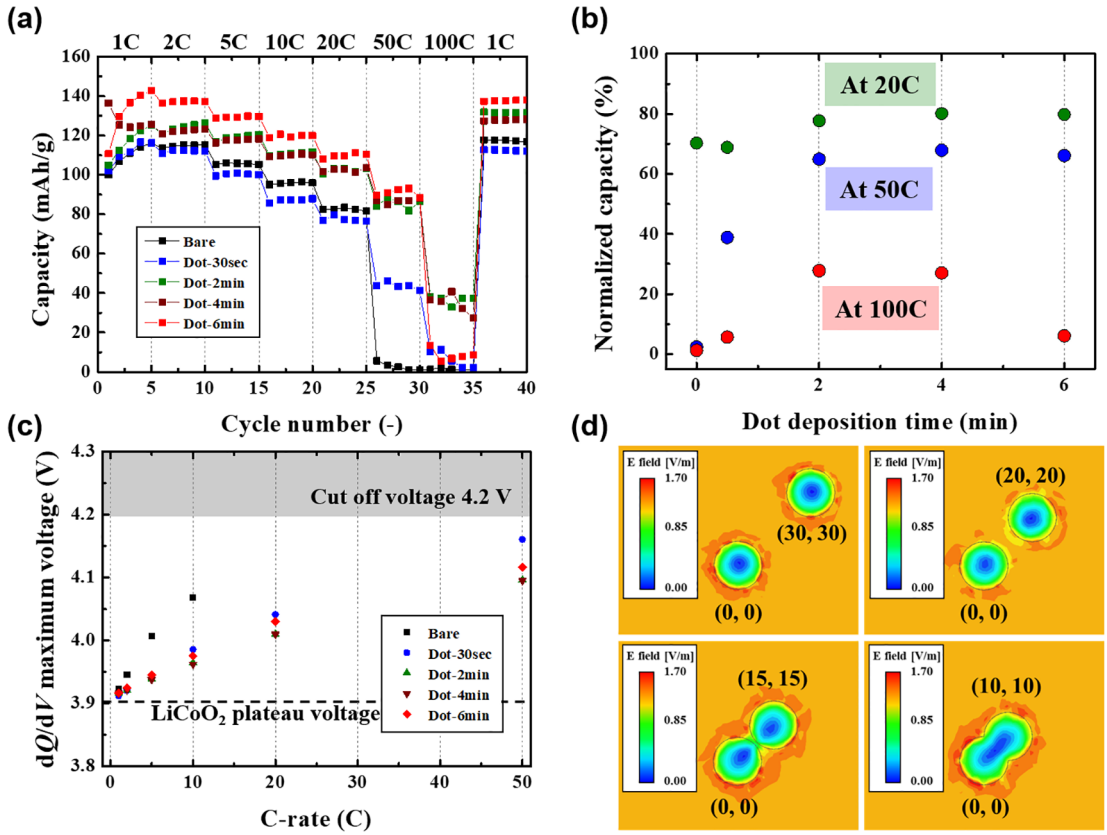

Fig. 3. Discharge capacities of Bare (black), Dot-30sec (blue), Dot-2 min (green), Dot-4 min (dark-red) and Dot-6 min (bright-red) (a). Normalized capacity at 50C and 100C *vs.* dot deposition time (b). dQ/dV maximum voltage *vs.* C-rate (c). Calculated electric field mappings with two dots deposited on LCO surface (d). (For interpretation of the references to colour in this figure legend, the reader is referred to the web version of this article.)

of the interface between electrode and electrolyte where insertion/deinsertion into/from LCO occurs is decreasing, as with increased surface coverage (Fig. 2f).

In the case of high surface coverage, Li^+ underneath the BTO dots must diffuse along the in-plane direction of LCO during charging/discharging, and Li^+ can de-intercalate to electrolyte from the electrode at only TPI. The diffusion coefficient of LCO, D_{Li}, was reported to be around 1.0×10^{-12} cm^2/s [17]. Considering D_{Li}, the maximum inner diffusion length of Li^+ in LCO would be less than 30 nm at 50C, and 10 nm at 100C. If the rate-limiting step is the inner diffusion process,

the discharge capacity should follow the TPI length (shown in Fig. 2g), and thus Dot-6 min should show a larger discharge capacity than Dot-2 min, because the TPI length of Dot-6 min is longer. However, Dot-6 min alone showed a worse performance at 100C. These results indicate that the rate-limiting step of Dot-6 min at 100C is not caused by the inner diffusion process.

The normalized discharge capacity of Dot-6 min at 100C could not be explained by the inner diffusion step in LCO. We then calculated the electric field maps of the LCO surface with two BTO dots on LCO using ANSYS-HFSS. Details of the experimental procedure may be found in our previous report [11]. The dielectric constant of BTO and SEI were set as 100 and 10, respectively. One BTO dot with 10 nm radius was put in the original position (0, 0) and the other on the position (x, y). We calculated four (x, y) positions (30, 30), (20, 20), (15, 15) and (10, 10) in nm unit. The results are shown in Fig. 3(d). The dots showed no interactions in the case of (x, y) (30, 30), and the electric field concentration was observed around each dot. However, as each dot approached, the electric field at the area between two dots was relatively weakened. In the case where (x, y) (10, 10), the dots are coalescing, the two dots behave as if one, and the electric field concentration could be observed along the circumference. These results indicate that increasing the number of dots reduced the dot-dot distance, and consequently, the electric field at TPI would be weakened at the inter-area of two dots even if they do not coalesce. The dots interaction decreases electric field concentration at TPI between two dots when two dots take less than 10-nm distance from edge to edge in the calculation. Here, considering the case of Dot-6 min, there are quit high concentration of BTO dots and several dots should coalescent (Fig. 2(f, g)). As following the dots interaction, the electric field concentration should be weak when two dots take quit few distance or coalescent. In that case, the electric field concentrated area would decrease. Moreover, we infer that dots interaction would vary with the C-rate. Therefore, the Li^+ migration between electrode and electrolyte interfaces could not be improved at the inter-area of two dots, and this dots interaction can explain that Dot-6 min could work at 50C, but not at 100C.

4. Conclusion

In this study, we investigated the dependence of surface $BaTiO_3$ nanodot density on high C-rate performance using epitaxial $LiCoO_2$ thin film produced by pulsed laser deposition (PLD). As the surface supporting nanodots increased, the discharge capacity at 20C and 50C also increased to saturation at surface coverage over 22%. However, at 100C, the discharge capacity was decreased at surface coverage over 40%. These results indicate that coalescence of nanodots reduces not only the TPI length, but also the electrochemically active sites at quite high C-rate.

Declaration of Competing Interest

The authors declare that they have no known competing financial interests or personal relationships that could have appeared to influence the work reported in this paper.

Acknowledgments

This work was partly supported by JSPS KAKENHI Grants-in-Aid for Challenging Research (Pioneering) (M.I. 17H06240) and (Exploratory) (Sh.Y. 18K19126), Scientific Research (B) (S.Y. 19H02426, T.T. 18H01707), by the MEXT Elements Strategy Initiative to form Core Research Center, and Collaborative Research Project of Laboratory for Materials and Structures, and the Project of Creation of Life Innovation Materials for Interdisciplinary and International Researcher Development MEXT, Japan.

References

[1] J.-M. Tarascon, M. Armand, Nature 414 (2001) 359.
[2] J.B. Goodenough, Y. Kim, Chem. Mater. 22 (2010) 587.
[3] T. Ohzuku, A. Ueda, J. Electrochem. Soc. 141 (1994) 2972.
[4] E. Jeong, C. Hong, Y. Tak, S.C. Nam, S. Cho, J. Power Sources 159 (2006) 223.
[5] K.J. Griffith, A.C. Forse, J.M. Griffin, C.P. Grey, J. Am. Chem. Soc. 138 (2016) 8888.
[6] K.J. Griffith, K.M. Wiaderek, G. Cibin, L.E. Marbella, C.P. Grey, Nature 559 (2018) 556.
[7] M. Okubo, E. Hosono, J. Kim, M. Enomoto, N. Kojima, T. Kudo, H. Zhou, I. Honma, J. Am. Chem. Soc. 129 (2007) 7444.
[8] I.D. Scott, Y.S. Jung, A.S. Cavanagh, Y. Yan, A.C. Dillon, S.M. George, S.-H. Lee, Nano Lett. 11 (2011) 414.
[9] T. Teranishi, Y. Yoshikawa, R. Sakuma, H. Hashimoto, H. Hayashi, A. Kishimoto, T. Fujii, Appl. Phys. Lett. 105 (2014) 143904.
[10] T. Teranishi, N. Katsuji, K. Chajima, S. Yasuhara, M. Inohara, Y. Yoshikawa, S. Yasui, H. Hayashi, A. Kishimoto, M. Itoh, Adv. Electron. Mater. 4 (2018) 1700413.
[11] S. Yasuhara, S. Yasui, T. Teranishi, K. Chajima, Y. Yoshikawa, Y. Majima, T. Taniyama, M. Itoh, Nano Lett. 19 (2019) 1688.
[12] S. Yasuhara, S. Yasui, T. Teranishi, Y. Yoshikawa, T. Taniyama, M. Itoh, J. Power Sources 441 (2019) 227194.
[13] T. Ohnishi, K. Takada, Appl. Phys. Express 5 (2012) 055502.
[14] T. Ohnishi, B.T. Hang, X. Xu, M. Osada, K. Takada, J. Mater. Res. 25 (2010) 1886.
[15] J. Yan, J. Zhang, Y.-C. Su, X.G. Zhang, B.-J. Xia, Electrochem. Acta 55 (2010) 1785.
[16] S.J. An, J. Li, C. Daniel, D. Mohanty, S. Nagpure, D.L. Wood, Carbon 105 (2016) 52.
[17] S. Takeuchi, H. Tan, K.K. Bharathi, G.R. Stafford, J. Shin, S. Yasui, I. Takeuchi, L.A. Bendersky, ACS Appl. Mater. Interfaces 7 (2015) 7901.